tvst

https://doi.org/10.1167/tvst.7.6.42

Article

Comparative Optical Coherence Tomography Angiography of Wild-Type and rd10 Mouse Retinas

Tae-Hoon Kim[1], Taeyoon Son[1], Yiming Lu[1], Minhaj Alam[1], and Xincheng Yao[1,2]

[1] Department of Bioengineering, University of Illinois at Chicago, Chicago, IL, USA
[2] Department of Ophthalmology and Visual Sciences, University of Illinois at Chicago, Chicago, IL, USA

Correspondence: Xincheng Yao, University of Illinois at Chicago, Bioengineering and Ophthalmology, Clinical Sciences North, Suite W103, Room 164D, 820 S Wood Street, Chicago, IL 60612, USA. e-mail: xcy@uic.edu

Received: 11 July 2018
Accepted: 2 November 2018
Published: 28 December 2018

Keywords: optical coherence tomography; retinal vasculature; retinal degeneration; retinitis pigmentosa; rd10

Citation: Kim T-H, Son T, Lu Y, Alam M, Yao X. Comparative optical coherence tomography angiography of wild-type and rd10 mouse retinas. Trans Vis Sci Tech. 2018;7(6):42, https://doi.org/10.1167/tvst.7.6.42

Purpose: To conduct longitudinal optical coherence tomography angiography (OCTA) to characterize dynamic changes of trilaminar vascular plexuses in wild-type (WT) and retinal degeneration 10 (rd10) mouse retinas.

Methods: Longitudinal in vivo OCT/OCTA measurements of WT and rd10 mouse retinas were conducted at postnatal day 14 (P14), P17, P21, P24, and P28. OCT images were used to quantify retinal thickness changes, while OCTA images were used to investigate vascular dynamics within the trilaminar vascular plexuses, that is, superficial vascular plexus (SVP), intermediate capillary plexus (ICP), and deep capillary plexus (DCP). Blood vessel densities of all three plexus layers were quantitatively evaluated separately. The caliber of first-order blood vessel branches in the SVP layer was also measured.

Results: Vascular densities in all three plexuses continuously decreased with aging in both WT and rd10. However, abnormal density reduction in rd10 occurred at P17 in both ICP ($P < 0.001$) and DCP ($P < 0.001$). While the ICP of rd10 showed density recovery at P24, the DCP of rd10 showed significantly low density. Remarkable vascular narrowing in rd10 was also observed in the SVP, especially at P28.

Conclusions: The most severe vascular impairment happened in the DCP, while the ICP showed the transient recovery of vascular density after the onset of retinal degeneration. The SVP was most resistant to the retinal degeneration, but the first-order blood vessel branches within the SVP showed progressive narrowing.

Translational Relevance: Better understanding of the vascular changes correlated with retinal development, and retinal degeneration can provide insights in advanced development of treatment protocols of retinal degenerative diseases.

Introduction

Retinitis pigmentosa (RP) is a hereditary and genetically heterogeneous retinal disorder.[1] RP is characterized by the progressive degeneration of rod photoreceptors that usually begins in the mid-peripheral retina and spreads to the peripheral retina.[2] The rod degeneration causes night blindness as an early symptom and gradually constricts the visual field, and ultimately results in complete blindness due to subsequent loss of cone photoreceptors.[3] Clinical indications of RP are abnormal a- and b-waves in electroretinogram (ERG), intraretinal clumps of black pigment in fundus image, retinal thinning, dust-like particles in the vitreous, and reduced visual field.[4] It is known that the retina is a complex neurovascular network, and retinal neural degeneration in RP is strongly accompanied with retinal vascular distortion. The hallmarks are reduced vascular density,[5–7] vascular narrowing,[4,8] vascular sclerosis,[9,10] and reduced blood flow.[11–13] Longitudinal monitoring of vascular viability is of great importance to follow-up the progress of therapeutic interventions.[14,15]

Retinal degeneration 10 (rd10) mouse is a widely used autosomal recessive RP model, which carries a spontaneous missense point mutation in PDE6B (cGMP phosphodiesterase 6B, rod photoreceptor), presenting in approximately 5% of RP patients.[3,16] Depth-resolved OCT of rd10 mice revealed a

progressive decline in outer retinal thickness,[17] while there was no detectable change in inner retinal thickness in rd10 mice with aging.[18] The presence of hyperreflective opacities in the vitreous was also reported in rd10 mice.[17] Another OCT study observed a shallow serous retinal detachment at around 3 weeks old and a vanished ellipsoid zone with aging.[19]

Rd10 mice provide an efficient time frame to conduct in vivo investigation of pathological mechanisms and treatment protocols of RP. Rd10 mice start to open eyes at around postnatal day 12 (P12), and progressive retinal degeneration starts at around P16, and maximum cell death occurs between P21 and P25.[16,20–22] Retinal neural and vascular developments are known to complete within 3 weeks in mice.[8,14] In other words, a big wave of retinal neurovascular development and degeneration occurs within a short time window between P14 to P28. However, there is a lack of in vivo study for longitudinal monitoring of progressive retinal neurovascular degeneration in rd10 during this specific time window. This limits our understanding of neurodegenerative effects on dynamical changes of vascular functionality in rd10 retina.

As a new OCT imaging modality, OCT angiography (OCTA) can provide noninvasive visualization of retinal and choroidal vasculatures.[23] Previous OCTA studies have successfully demonstrated stimulus evoked hemodynamic responses in individual retinal layers,[24] laser-induced choroidal neovascularization,[25,26] retinal vascular occlusions produced by laser photocoagulation,[27] and assessments of retinal and choroidal vasculatures in an oxygen-induced retinopathy model.[28]

We have recently demonstrated in vivo functional OCT[29] and OCTA[24,30] of retinal physiology in wild-type (WT) mice. In this study, we aim to validate comparative OCT/OCTA of WT and rd10 mice to investigate longitudinal vascular property correlated with retinal development and degeneration. By providing three-dimensional (3D) imaging capability, in vivo OCTA observation of longitudinal dynamics of trilaminar vascular plexuses, that is, the superficial vascular plexus (SVP), the intermediate capillary plexus (ICP), and the deep capillary plexus (DCP),[31,32] was conducted. Quantitative OCTA measurements of retinal vascular properties of WT and rd10 mice were implemented at five longitudinal time points, that is, P14, P17, P21, P24, and P28.

Methods

Animals

This study followed the Association for Research in Vision and Ophthalmology Statement for the Use of Animals in Ophthalmic and Vision Research. All experiments were performed following the protocols approved by the Animal Care Committee at the University of Illinois at Chicago. WT mice (C57BL/6J; The Jackson Laboratory, Bar Harbor, ME) from three different litters ($n = 13$: 8 males, 5 females) and rd10 mice (homozygous for the Pde6b^{rd10} on C57BL/6J background; The Jackson Laboratory) from four different litters ($n = 16$: 7 males, 9 females) were used in this study. The mice were reared in a 14/10-hour light/dark cycle.

OCT/OCTA System

A custom-designed OCT/OCTA system (Fig. 1) was used for this study. Technical details of the system are reported in our previous publication.[24] Briefly, a near infrared super-luminescent diode (SLD) with a central wavelength $\lambda = 850$ nm and a bandwidth $\Delta\lambda = 100$ nm (D840, Superlum, Carrigtwohill, County Cork, Ireland) was used as the OCT light source. A line CCD camera (AViiVA EM4; e2v Technologies, Chelmsford, UK) was used in the custom-built OCT spectrometer, and the frame speed of the camera was set to a 30-kHz A-scan rate for this study. The axial and lateral resolutions of the system were theoretically estimated at 3 and 12 μm, respectively. The axial resolution was experimentally measured at 3.3 μm, which allows visualizing blood vessels at individual capillary level resolution.[24] The depth of field (DOF) was set to 300 μm, and the light power illuminated on the mouse cornea was set to 0.95 mW.

Experiment Procedures

Longitudinal OCT/OCTA measurements were conducted at P14, P17, P21, P24, and P28. The retinal OCT and OCTA images were obtained in a laboratory room under ambient light condition. An awake mouse was first placed in a container and body weight was measured for dose estimation of anesthesia. Anesthesia was intraperitoneally induced by a mixture of 60 mg/kg ketamine and 3 mg/kg xylazine. To access full aperture of the small pupil of mouse pups, a drop of ophthalmic mydriatic (1% atropine sulfate ophthalmic solution; Akorn, Lake

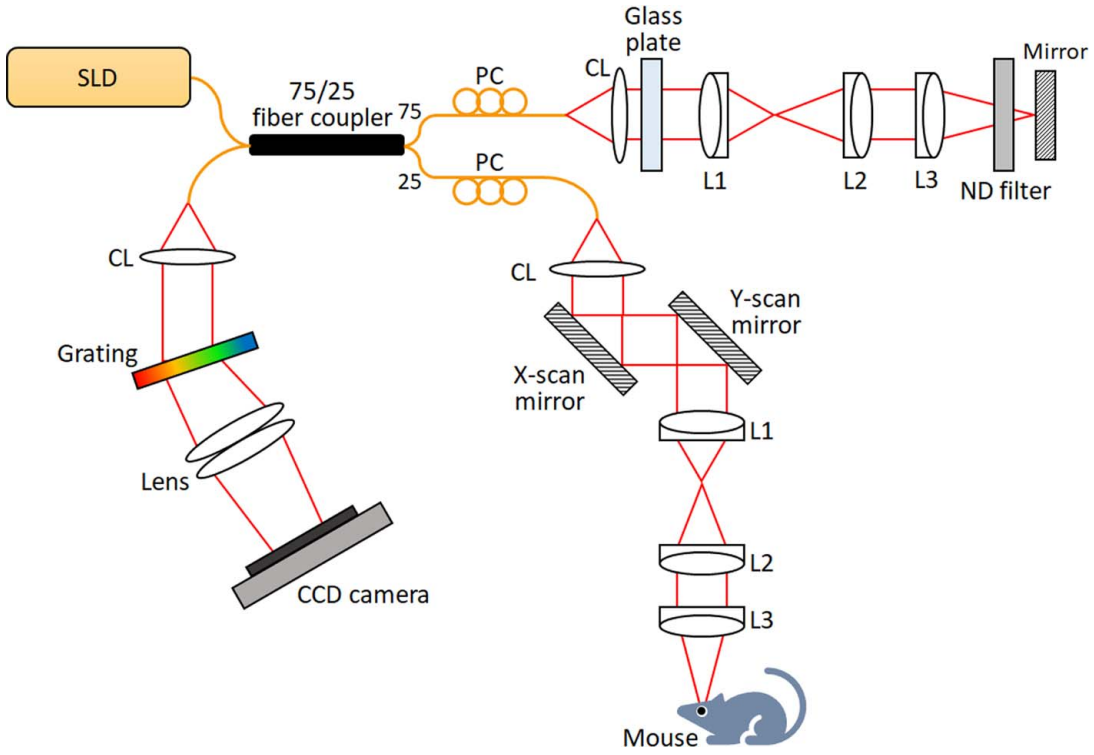

Figure 1. Optical diagram of the OCT/OCTA setup. CL, collimation lens; L1, L2, L3, lens; PC, polarization controller; SLD, super luminescent diode ($\lambda = 850$ nm).

Forest, IL) was applied to the left eye of mice where imaging was performed. Then, the mouse was placed to the custom-designed animal holder, with integrated bite bar and ear bar to minimize motion artefacts.[29] A cover glass (12-545-80; Microscope cover glass, Fisherbrand, Waltham, MA) along with a drop of eye gel (Severe; GenTeal, Novartis, Basel, Switzerland) was placed on the tested eye to compensate for optical aberrations of the mouse eye for resolution improvement.[33] After the mouse was fully anesthetized, the mouse head was fixed for OCT/OCTA recording. During the experiment, a heating pad was wrapped around the animal holder to keep the mouse warm.

Image Acquisition

Three-dimensional OCT/OCTA volume was acquired over 1.2 × 1.2 mm retinal region. Each acquired volume consisted of 500 B-scans and each B-scan consisted of 500 A-scans. Five repeated OCT B-scans were acquired at each position to compute speckle variances (SV) for OCTA construction.[24] Therefore, a total of 5 × 500 × 500 A-scans was acquired for each OCTA volume. We set a region of interest (ROI) covering the half of the optic nerve head (ONH) in the dorsal direction to keep tracking vascular changes in the same area for all mice.

Image Processing

Figure 2A illustrates the flow chart of image processing procedures for vascular density analysis of each plexus layer in the OCTA images. First, the OCT images were constructed with Fourier transform of the acquired raw spectrum. Second, the OCTA images were constructed by implementing SV processing of the OCT images.[24] Third, bulk motion was corrected by image registration among sequential B-scans. This image registration was based on the vertical position tracing of the bottom edge of the hyperreflective OCT band of retinal pigment epithelial (RPE)/choroid complex, showing abrupt intensity changes. After the correction of bulk motion, both median filtering with a kernel size of 4×4 pixels and histogram equalization were applied for contrast enhancement of blood vessels (Fig. 2B1). Fourth, retinal flattening was conducted in each OCTA B-scan by using "Straighten" function in Fiji software (Fig. 2B2). Fifth, trilaminar segmentation was then manually conducted; the SVP (retinal nerve fiber layer [RNFL]/ganglion cell

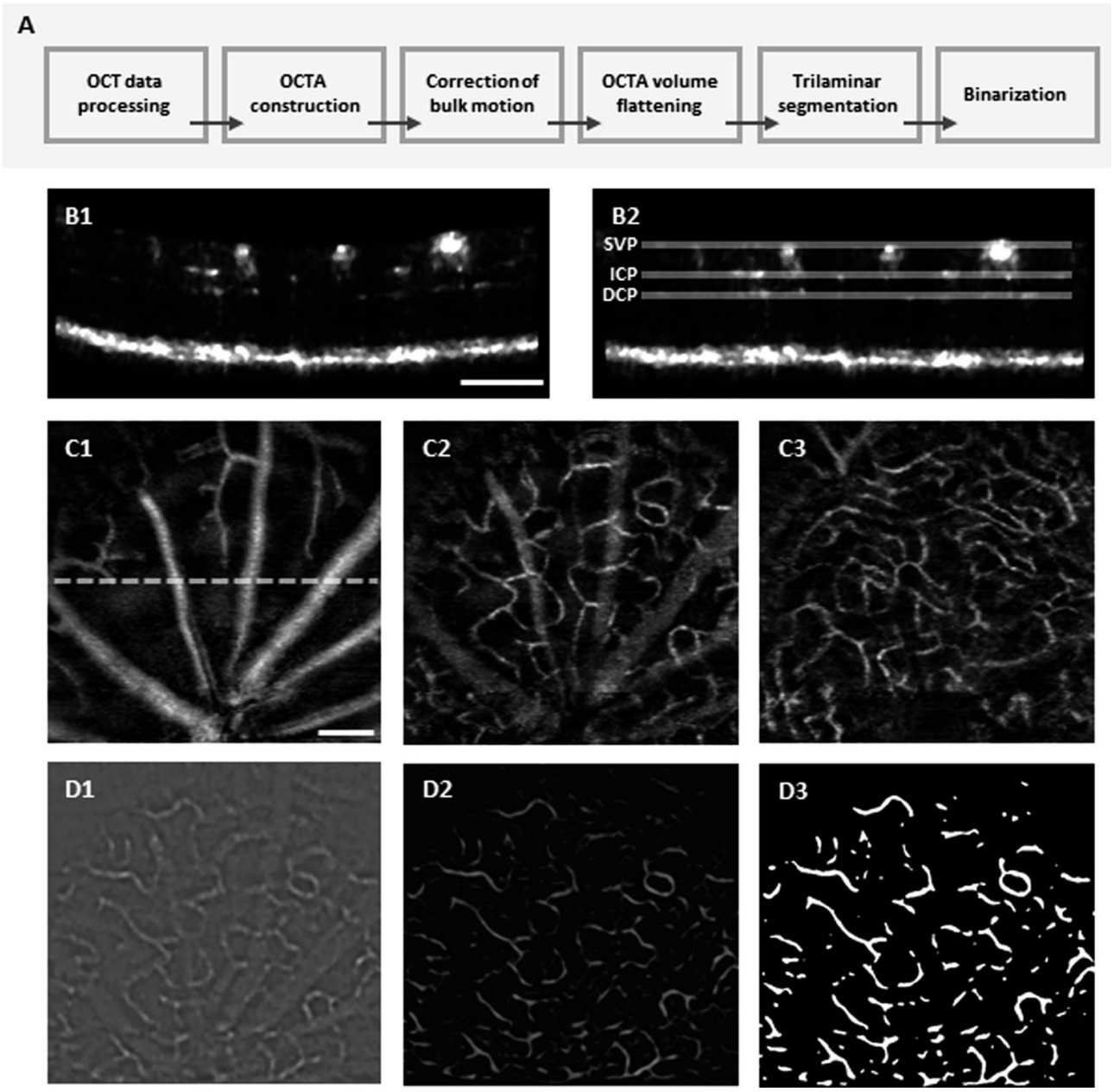

Figure 2. (A) Flow chart of image processing procedures. (B) Representative OCTA B-scan before (B1) and after (B2) flattening. (C) Representative en face images of segmented SVP (C1), ICP (C2), and DCP (C3) from a WT mouse at P24. A *dashed line* in C1 represents the B-scan position of B1 and B2. (D) Image binarization processing prepared for quantitative density analysis. A spatial bandpass filtering was applied to mitigate projection artifacts in the ICP (D1). For contrast enhancement, adaptive histogram equalization was applied (D2) and then binarization (D3) was realized. *Scale bar*: 200 μm.

layer), ICP (inner plexiform layer/inner nuclear layer), and DCP (outer plexiform layer) were individually segmented with 8 μm (5 pixels) thickness. For each plexus layer, a corresponding en face OCTA image was reconstructed by a maximum intensity Z-projection method (Figs. 2C1–2C3). Sixth, binarization processing was conducted to each en face OCTA image. For reliable binarization of the segmented image, a spatial bandpass filtering, which suppress objects size larger (down to 12 pixels) and smaller (up to 7 pixels) than blood vessels, was applied to the ICP and DCP to mitigate projection artifacts (Fig. 2D1). Background noise was subsequently corrected by using a "Rolling ball" algorithm in Fiji software. The radius of Rolling ball was set to 20 pixels for the SVP and 8

pixels for the ICP and DCP. And adaptive histogram equalization was applied to the image for contrast enhancement (Fig. 2D2). Binarization was realized by IsoData automatic method of threshold determination[34] and the binarized image was further processed by morphological opening operation with a 2×2 pixels square structuring element to remove small particle noises (Fig. 2D3). All input parameters used in the image processing were first experimentally determined based on qualitative optimization and applied to the all data sets. Image processing was performed with a custom developed software package based on MATLAB R2016a (MathWorks, Natick, MA), in coordination with image processing package available in Fiji software (http://fiji.sc/Fiji).

Data Analysis

Total retinal thickness was measured from RNFL to RPE layer, and outer retinal thickness was also measured from outer nuclear layer (ONL) to RPE in the OCT B-scan. The location measured was 650 μm dorsally away from the ONH, which was also the central line of the ROI. The thickness was averaged over six A-lines along a B-scan. The vascular density for each layer was defined as the percentage of area occupied by vessels in the projection OCTA images after binarization. Mean calibers of the first-order blood vessel branches in the SVP were also measured. The measurement area was confined to the lower end (one-third part of the SVP image), and triple times measurements were implemented per each vessel to minimize observation error. All data are expressed as mean ± standard deviation (SD) per group. Pairwise comparison between the WT and rd10 groups was performed using Student's *t*-tests (equal variances) or Welch's *t*-tests (unequal variances), and $P < 0.05$ was considered statistically significant. For the vascular density analysis, a 1-way repeated measures ANOVA was additionally performed to compare the vascular density within each group over different time points. If a significant density variation was found, Tukey's HSD post hoc analyses were used to identify differences between group means.

Results

For each experiment, we first recorded the body weight and retinal thickness since abnormal retinal thinning is a direct indication of RP progression.[35] Thirteen WT and 16 rd10 mice were used in this study. Two data sets from one WT and one rd10 at their P28 were excluded from data analysis due to cataract formation. Slight differences were observed in both initial weight (WT: 6.28 ± 0.95 g; rd10: 7.39 ± 0.39 g; $P < 0.01$) (Fig. 3A) and retinal thickness (WT: 184.73 ± 5.26 μm; rd10: 180.28 ± 2.58 μm; $P < 0.05$) (Fig. 3B) between WT and rd10 at P14. Significant retinal thinning occurred in rd10 from P17, compared to WT ($P < 0.0001$) (Fig. 3B). As shown in Figure 3C, the retinal thinning in rd10 primarily attributed to the declined outer retinal thickness due to photoreceptor degeneration.[17]

Figures 4 and 5 show representative longitudinal OCTAs of trilaminar vascular plexuses in the WT and rd10 mouse retinas, respectively. Basically, the functional vascular densities in all three plexuses continuously decreased with aging in both WT and rd10. However, abrupt vascular attenuations were observed in rd10, corresponding to retinal degeneration.

Unlike the retinal thinning, the vascular density at P14 had no significant difference between the two groups in all three plexuses. However, notable density reduction in rd10 occurred at P17 in both the ICP (WT: 15.84% ± 2.37%; rd10: 11.72% ± 3.04% for rd10; $P < 0.001$) and the DCP (WT: 18.86% ± 3.28%; rd10: 13.30% ± 4.07%; $P < 0.001$) (Figs. 6B, 6C). Moreover, it was observed that the most vulnerable layer correlated with progressive retinal degeneration was the DCP, which was also clearly recognized in Figures 5C2 to 5C5. This may indicate low or absent blood flow in the DCP after P21 in rd10.

Figure 6 illustrates vascular densities in trilaminar vascular plexuses of WT and rd10 mouse retinas. For the SVP layer (Fig. 6A), the vascular density of the SVP steadily decreased with aging in both WT and rd10 groups, and their variation started being significant from P21 (WT: 30.06% ± 1.55%; rd10: 27.28% ± 1.73%; $P < 0.001$). Notable initial changes of the SVP density within each group occurred at P21 ($P < 0.001$) and at P17 ($P < 0.01$) in WT and rd10, respectively. For the ICP (Fig. 6B) and DCP (Fig. 6C) layers, significant vascular density difference between the WT and rd10 groups was recognized at P17 ($P < 0.001$). Moreover, retinal vascular density of the ICP in rd10 slightly increased at P24, compared to that at P17. This recovery was not observed in the DCP in rd10. Thus, it may indicate the presence of surviving inner retinal neurons (bipolar cells, horizontal cells, amacrine cells, and ganglion cells), still demanding high metabolism.[36] Notable initial changes of the ICP density within each group occurred at P21 ($P < 0.05$)

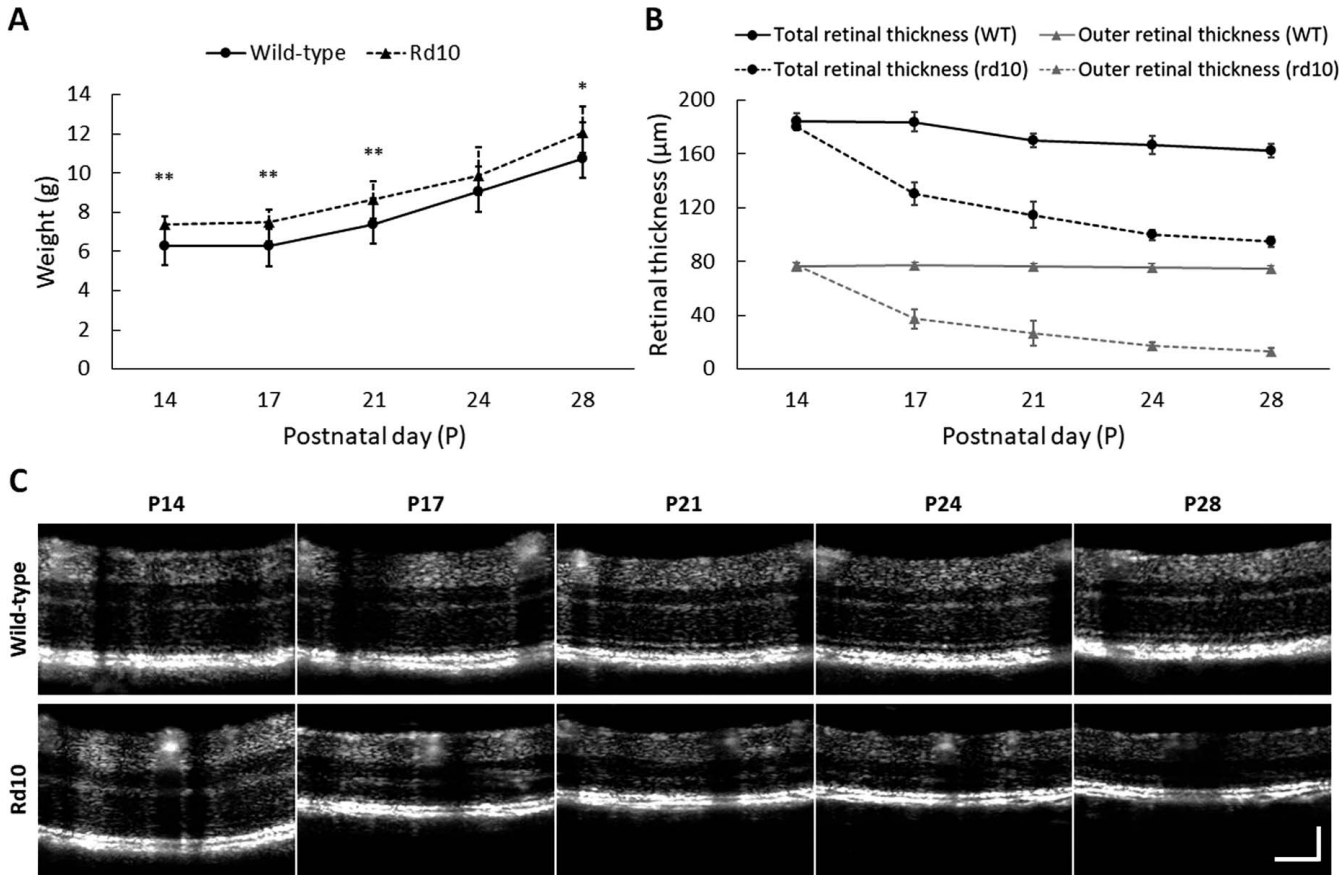

Figure 3. (A) Body weight information. Mean weight of WT and rd10 at P14 was 6.28 ± 0.95 g and 7.39 ± 0.39 g, respectively, and the mean weight increased to 10.77 ± 1.82 g (WT) and 12.05 ± 1.33 g (rd10) at P28. (B) Retinal thickness information. Rd10 showed dramatic thinning of total retinal thickness preceded by the onset of retinal degeneration: 180.3 ± 2.58 μm (P14), 130.2 ± 10.61 μm (P17), 114.8 ± 14.97 μm (P21), 99.9 ± 3.71 μm (P24), and 94.7 ± 3.50 μm (P28). Rd10 showed significant decrease of outer retinal thickness with aging: 74.45 μm (P14) and 13.33 μm (P28), while the thickness of WT only slightly decreased with aging: 76.38 μm (P14) and 73.04 μm (P28). (C) OCT B-scan images averaged over 30 images. The location of this B-scan was 650 μm dorsally away from ONH, and the retinal thickens was measured from RNFL to RPE. *Scale bar*: 100 μm. $N = 13$ for WT and $N = 16$ for rd10. P values for pairwise comparisons between WT and rd10 are indicated by *asterisks*: *$P < 0.05$; **$P < 0.01$; ***$P < 0.001$; ****$P < 0.0001$.

and at P17 ($P < 0.01$) in WT and rd10, respectively, and that of the DCP density only occurred within rd10 group at P17 ($P < 0.0001$).

Figure 7 illustrates quantitative measurement of blood vessel caliber. Remarkable vascular narrowing in rd10 was also observed especially at P28. In order to quantify the vascular narrowing, we measured mean vessel calibers for the first-order blood vessel branches in the confined area (Fig. 7A). Figure 7B shows that the mean difference was recognized at P21 (WT: 23.17 ± 6.50 pixels; rd10: 21.72 ± 4.36 pixels; $P < 0.01$) and it was further segregated over time between two groups ($P < 0.0001$ at P 24, $P < 0.0001$ at P 28). At P14, we also noticed that the mean vessel caliber in rd10 was thicker than WT at P14 (WT: 22.53 ± 6.83 pixels; rd10: 23.91 ± 6.52 pixels; $P < 0.05$).

Discussion

We report here the first time in vivo longitudinal OCTA observation of retinal degeneration associated vascular distortions in three individual vascular plexuses, that is, SVP, ICP, and DCP layers in rd10 mouse retinas. Comparative OCTA of WT and rd10 mice confirmed that the retinal vasculature in rd10 retina was significantly impaired within a short time period due to retinal degeneration. Different aspects of vascular degeneration were observed in the DCP, ICP, and SVP.

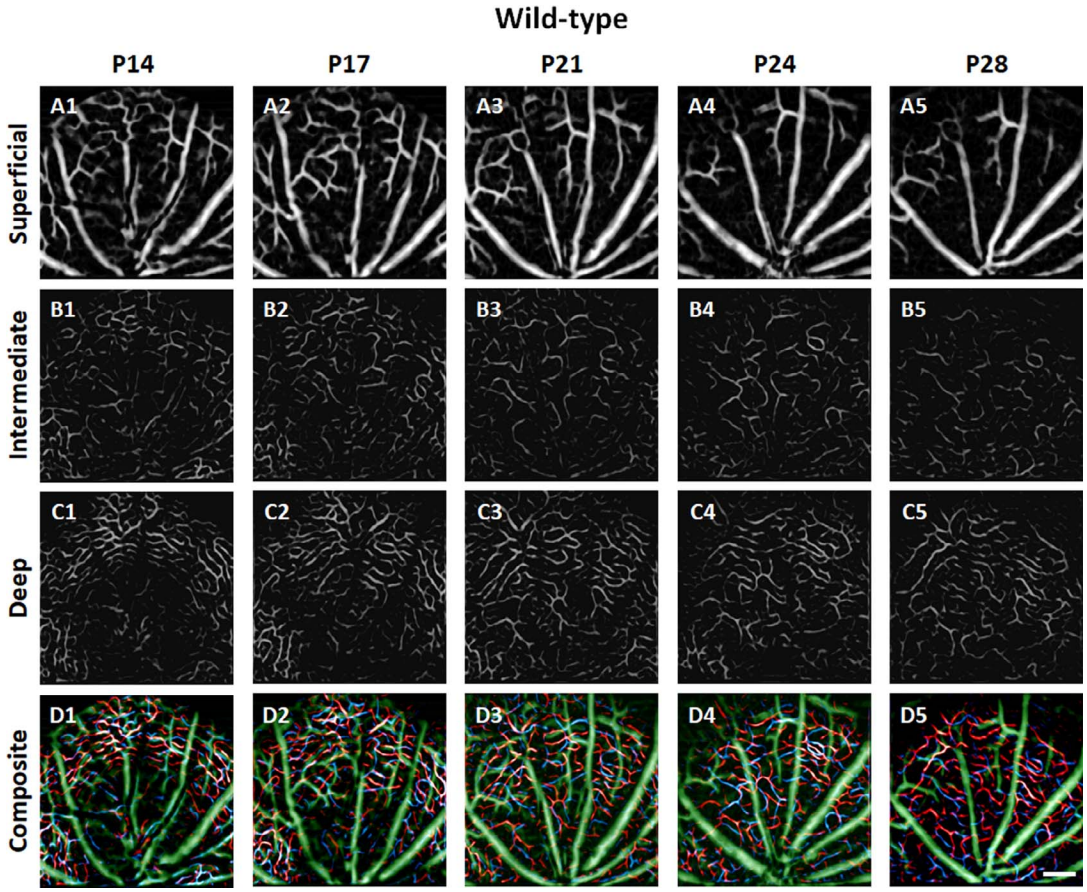

Figure 4. Representative OCTA images of SVP (A), ICP (B), and DCP (C) in WT mouse retinas recorded at P14, P17, P21, P24, and P28. In the composite OCTA images (D), *green*, *blue*, and *red* colors represent the superficial, intermediate, and deep plexuses, respectively. *Scale bar*: 200 μm.

We found not only significant retinal thinning in the outer retina of rd10 with aging due to retinal degeneration, but also the initial difference of retinal thickness between WT and rd10. This difference might result from the initial weight difference between two groups (Fig. 3A). A study reported that ocular stretching as the mice physically grew up naturally induced retinal thinning.[37] Accordingly, WT showed the decreasing retinal thickness during initial development as shown in Figure 3B. This result is consistent with recent in vivo OCT study of mouse retinas.[17,18,38]

The DCP was most attenuated among the three plexuses in rd10, which is consistent with the previous observations of clinical and animal research of RP.[39–41] The rationale behind the severe attenuation of the DCP has been proposed by hyperoxia in the retina.[42–47] A study demonstrated that the loss of photoreceptor metabolism allows oxygen from the choroidal vasculature to reach the inner retina, thereby attenuating retinal circulation via oxygen vasoconstriction.[44] It was also demonstrated that accelerated retinal photoreceptor apoptosis induced an extracellular hyperoxygenation.[45,46] Another study demonstrated that it was able to reverse the DCP density of nearly 100% preceded by the loss of the photoreceptors in the transgenic mice by placing the mice in an ambient hypoxic environment.[47]

The ICP showed unambiguous recovery of vascular density after P21 in rd10. It may reflect rescued neural activities of the inner retina against the photoreceptor degeneration. It was reported that the inner retinal layers underwent extensive remodeling,[22] and about 20% of bipolar cells were lost between 1.5 and 3.5 months[21] in rd10 mice. It was also demonstrated that the remodeling primarily occurred in bipolar and horizontal cells by progressive dendritic retraction and loss of synaptic connections followed by glial and amacrine cell remodeling.[48–50] Such remodeling was also observed in RP patients.[51] Although the attenuation rate of the ICP was slower than the DCP, the inner retinal part also ultimately

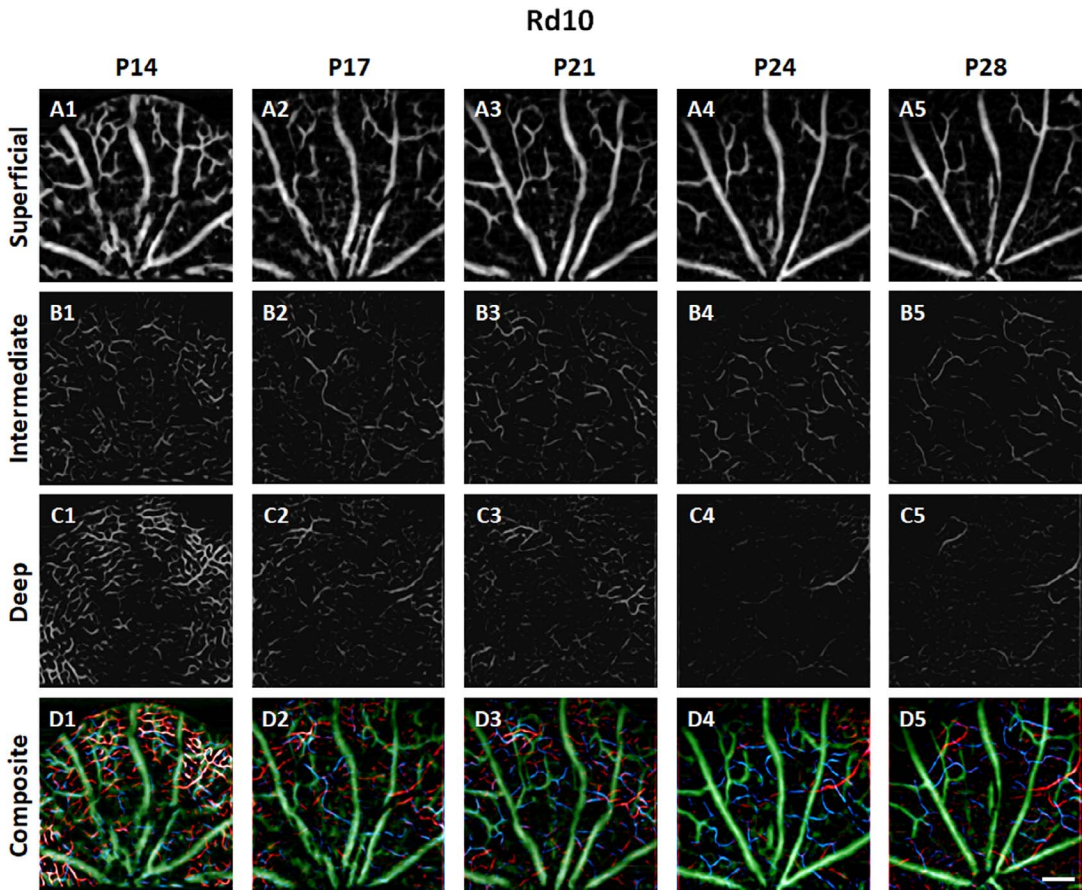

Figure 5. Representative OCTA images of SVP (A), ICP (B), and DCP (C) in rd10 mouse retinas recorded at P14, P17, P21, P24, and P28. In the composite OCTA images (D), *green*, *blue*, and *red* colors represent the superficial, intermediate, and deep plexuses, respectively. *Scale bar*: 200 μm.

degenerates with a delayed time course compared to early photoreceptor degeneration,[52] accompanying retinal vascular degeneration in the ICP.

The SVP was the least sensitive area to the retinal degeneration. Previous research[53] reported that the retinal ganglion cell (RGC) layer was resistant to both outer and inner retinal neural loss, and photoreception was still possible in a retina with significant neural degeneration. Based on a single-cell approach analysis, a previous study demonstrated that the

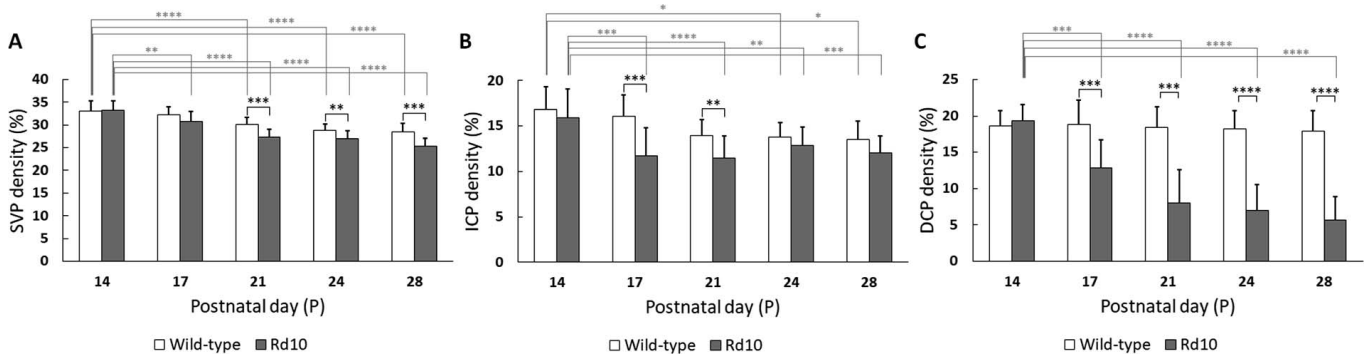

Figure 6. Comparative results of functional vascular density in trilaminar vascular plexuses. The vascular density was defined as the percentage of area occupied by vessels in the projection OCTA images. (A) SVP, (B) ICP, and (C) DCP. $N = 13$ for WT and $N = 16$ for rd10. *P* values for statistical significances are indicated by *asterisks*: *$P < 0.05$; **$P < 0.01$; ***$P < 0.001$; ****$P < 0.0001$.

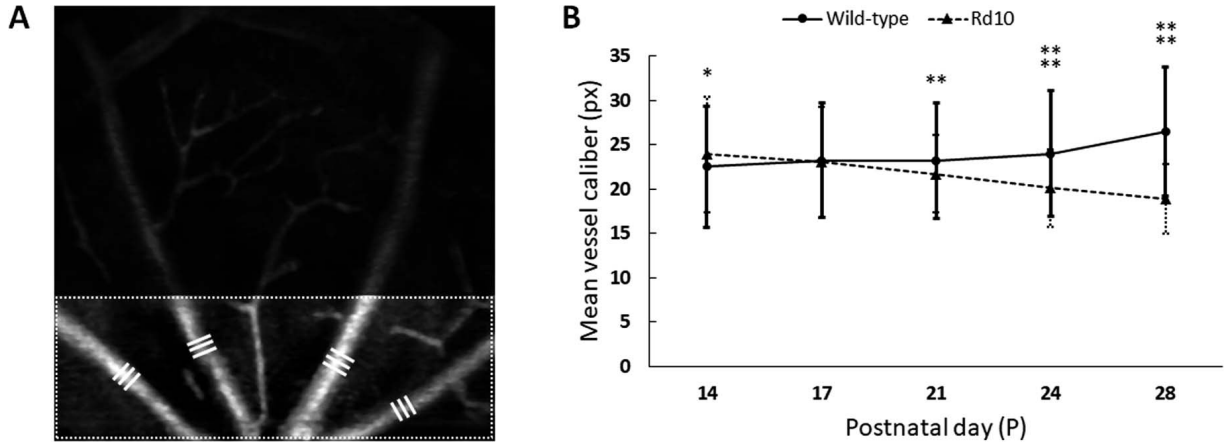

Figure 7. Quantitative measurement of blood vessel caliber. (A) Mean calibers of the first-order blood vessel branches in the SVP were measured. The measurement area was confined to the lower end (one-third part of the SVP image), and triple times measurements (*white bars*) were made per each branch. (B) With aging, mean vessel caliber increased in WT (22.5 ± 6.83 pixels at P14 to 26.5 ± 7.29 pixels at P28), while it decreased in rd10 (23.9 ± 6.52 pixels at P14 to 18.9 ± 3.93 pixels at P28). $N = 13$ for WT and $N = 16$ for rd10. P values for pairwise comparisons between WT and rd10 are indicated by *asterisks*: *$P < 0.05$; **$P < 0.01$; ***$P < 0.001$; ****$P < 0.0001$.

dendritic architecture and overall viability of all types of RGC in rd10 remained intact, even after complete photoreceptor degeneration and regressive remodeling of the inner retinal neurons up to 9 months of age.[54] However, we observed that the vascular density of the SVP between WT and rd10 groups showed significant difference from P21. Previous studies have revealed thickening of the blood vessel wall and following lumen occlusion led vessel narrowing and sclerosis in RP.[9,10] Therefore, we speculate that both capillary pruning and vascular narrowing are the causes of the observed vascular density reduction.

In addition, we found that the vascular density in the SVP of WT also steadily decreased with aging, while the mean vessel caliber increased during retinal development. In the SVP of WT, the reduced number of total blood vessel branches by pruning of capillaries as a process of vascular development might be a dominant factor in computing the vascular density rather than the vascular thickening.[55] We also observed that the SVP density was higher than the ICP and DCP density. Previous OCTA[56] and fluorescence angiography[57] reported higher vascular density in the deep vascular plexus (DVP) compared to the SVP in mouse retinas. This is not conflict to our observation, since we differentiated the DVP into two separate layers, that is, ICP and DCP, for quantitative analysis. If we consider the overall density of the ICP and DCP, it will be higher than that of the SVP.

There are a few limitations in this present study. First, the vessel area of the retinal vasculatures, particularly micro capillary level structures, might be overestimated due to the limited lateral resolution of our OCTA system.[58] Another limitation is projection artifact. Although a spatial bandpass filter was applied to the segmented en face images of the ICP and DCP to mitigate the shadow artifacts originated from main arteries and veins in the SVP, other projection artifacts originated from residual hyaloid vessels in the vitreous of younger pups (P14 and P17) made local regions void and may lead to lower vessel densities in all three plexus layers.[28,57] Moreover, accurate registration of blood vessels in the projection images over different time points was difficult in this study due to dynamic changes of vascular density and morphological features under the pruning process during retinal development.

Conclusion

In summary, we demonstrated the feasibility of in vivo longitudinal OCTA monitoring of trilaminar vascular changes in the WT and rd10 mice. In the rd10 mice, the DCP showed the most severe attenuation, while the ICP showed unambiguous recovery of vascular density after the onset of retinal degeneration. The SVP was most resistant to the retinal degeneration, but the first-order blood vessel branches showed progressive narrowing associated with retinal neural degeneration. We anticipate that the OCTA will allow longitudinal monitoring and quantitative assessment of therapeutic interventions in the rd10, other animal models, and human subjects, promising a valuable tool for better study of disease

mechanism and advanced development of treatment protocols.

Acknowledgments

This research was supported in part by NIH grants R01 EY023522, R01 EY024628, P30 EY001792; by and unrestricted grant from Research to Prevent Blindness; and by Richard and Loan Hill endowment.

Disclosure: **T.-H. Kim**, None; **T. Son**, None; **Y. Lu**, None; **M. Alam**, None; **X. Yao**, None

References

1. Veltel S, Gasper R, Eisenacher E, Wittinghofer A. The retinitis pigmentosa 2 gene product is a GTPase-activating protein for Arf-like 3. *Nat Struct Mol Biol*. 2008;15:373–380.
2. Ferrari S, Di Iorio E, Barbaro V, Ponzin D, Sorrentino FS, Parmeggiani F. Retinitis pigmentosa: genes and disease mechanisms. *Curr Genom*. 2011;12:238–249.
3. Hartong DT, Berson EL, Dryja TP. Retinitis pigmentosa. *Lancet*. 2006;368:1795–1809.
4. Fahim AT, Daiger SP, Weleber RG. Nonsyndromic retinitis pigmentosa overview. In: Adam MP, Ardinger HH, Pagon RA, et al., eds. *GeneReviews*. Seattle, WA: University of Washington, Seattle; 1993–2018 (2000; updated 2017). Retrieved from https://www.ncbi.nlm.nih.gov/books/NBK1417/
5. Battaglia Parodi M, Cicinelli MV, Rabiolo A, et al. Vessel density analysis in patients with retinitis pigmentosa by means of optical coherence tomography angiography. *Br J Ophthalmol*. 2017;101:428–432.
6. Toto L, Borrelli E, Mastropasqua R, et al. Association between outer retinal alterations and microvascular changes in intermediate stage age-related macular degeneration: an optical coherence tomography angiography study. *Br J Ophthalmol*. 2017;101:774–779.
7. Koyanagi Y, Murakami Y, Funatsu J, et al. Optical coherence tomography angiography of the macular microvasculature changes in retinitis pigmentosa. *Acta Ophthalmol*. 2018;96:e59–e67.
8. Otani A, Kinder K, Ewalt K, Otero FJ, Schimmel P, Friedlander M. Bone marrow-derived stem cells target retinal astrocytes and can promote or inhibit retinal angiogenesis. *Nature Med*. 2002;8:1004–1010.
9. Milam AH, Li ZY, Fariss RN. Histopathology of the human retina in retinitis pigmentosa. *Prog Retin Eye Res*. 1998;17:175–205.
10. Li ZY, Possin DE, Milam AH. Histopathology of bone spicule pigmentation in retinitis pigmentosa. *Ophthalmology*. 1995;102:805–816.
11. Grunwald JE, Maguire AM, Dupont J. Retinal hemodynamics in retinitis pigmentosa. *Am J Ophthalmol*. 1996;122:502–508.
12. Akyol N, Kukner S, Celiker U, Koyu H, Luleci C. Decreased retinal blood flow in retinitis pigmentosa. *Can J Ophthalmol*. 1995;30:28–32.
13. Beutelspacher SC, Serbecic N, Barash H, et al. Retinal blood flow velocity measured by retinal function imaging in retinitis pigmentosa. *Graefes Arch Clin Exp Ophthalmol*. 2011;249:1855–1858.
14. Otani A, Dorrell MI, Kinder K, et al. Rescue of retinal degeneration by intravitreally injected adult bone marrow-derived lineage-negative hematopoietic stem cells. *J Clin Invest*. 2004;114:765–774.
15. Pang JJ, Dai X, Boye SE, et al. Long-term retinal function and structure rescue using capsid mutant AAV8 vector in the rd10 mouse, a model of recessive retinitis pigmentosa. *Mol Ther*. 2011;19:234–242.
16. Chang B, Hawes NL, Pardue MT, et al. Two mouse retinal degenerations caused by missense mutations in the beta-subunit of rod cGMP phosphodiesterase gene. *Vis Res*. 2007;47:624–633.
17. Pennesi ME, Michaels KV, Magee SS, et al. Long-term characterization of retinal degeneration in rd1 and rd10 mice using spectral domain optical coherence tomography. *Invest Ophthalmol Vis Sci*. 2012;53:4644–4656.
18. Rosch S, Johnen S, Muller F, Pfarrer C, Walter P. Correlations between ERG, OCT, and anatomical findings in the rd10 mouse. *J Ophthalmol*. 2014;2014:874751.
19. Hasegawa T, Ikeda HO, Nakano N, et al. Changes in morphology and visual function over time in mouse models of retinal degeneration: an SD-OCT, histology, and electroretinography study. *Jpn J Ophthalmol*. 2016;60:111–125.
20. Chang B, Hawes NL, Hurd RE, Davisson MT, Nusinowitz S, Heckenlively JR. Retinal degeneration mutants in the mouse. *Vis Res*. 2002;42:517–525.
21. Gargini C, Terzibasi E, Mazzoni F, Strettoi E. Retinal organization in the retinal degeneration

10 (rd10) mutant mouse: a morphological and ERG study. *J Comp Neurol*. 2007;500:222–238.
22. Barhoum R, Martinez-Navarrete G, Corrochano S, et al. Functional and structural modifications during retinal degeneration in the rd10 mouse. *Neuroscience*. 2008;155:698–713.
23. Spaide RF, Fujimoto JG, Waheed NK. Image artifacts in optical coherence tomography angiography. *Retina*. 2015;35:2163–2180.
24. Son T, Wang B, Thapa D, et al. Optical coherence tomography angiography of stimulus evoked hemodynamic responses in individual retinal layers. *Biomed Opt Exp*. 2016;7:3151–3162.
25. Liu W, Li H, Shah RS, et al. Simultaneous optical coherence tomography angiography and fluorescein angiography in rodents with normal retina and laser-induced choroidal neovascularization. *Opt Lett*. 2015;40:5782–5785.
26. Park JR, Choi W, Hong HK, et al. Imaging laser-induced choroidal neovascularization in the rodent retina using optical coherence tomography angiography. *Invest Ophthalmol Vis Sci*. 2016;57: Oct331–340.
27. Soetikno BT, Shu X, Liu Q, et al. Optical coherence tomography angiography of retinal vascular occlusions produced by imaging-guided laser photocoagulation. *Biomed Opt Exp*. 2017;8: 3571–3582.
28. Kim Y, Hong HK, Park JR, et al. Oxygen-induced retinopathy and choroidopathy: in vivo longitudinal observation of vascular changes using OCTA. *Invest Ophthalmol Vis Sci*. 2018; 59:3932–3942.
29. Wang B, Lu Y, Yao X. In vivo optical coherence tomography of stimulus-evoked intrinsic optical signals in mouse retinas. *J Biomed Opt*. 2016;21: 96010.
30. Son T, Alam M, Toslak D, Wang B, Lu Y, Yao X. Functional optical coherence tomography of neurovascular coupling interactions in the retina. *J Biophotonics*. 2018; e201800089.
31. Campbell JP, Zhang M, Hwang TS, et al. Detailed vascular anatomy of the human retina by projection-resolved optical coherence tomography angiography. *Sci Rep*. 2017;7:42201.
32. Zhi Z, Chao JR, Wietecha T, Hudkins KL, Alpers CE, Wang RK. Noninvasive imaging of retinal morphology and microvasculature in obese mice using optical coherence tomography and optical microangiography. *Invest Ophthalmol Vis Sci*. 2014;55:1024–1030.
33. Liu X, Wang CH, Dai C, Camesa A, Zhang HF, Jiao S. Effect of contact lens on optical coherence tomography imaging of rodent retina. *Curr Eye Res*. 2013;38:1235–1240.
34. Ridler TW, Calvard S. Picture thresholding using an iterative selection method. *IEEE Trans Syst Man Cyber*. 1978;8:630–632.
35. Sandberg MA, Brockhurst RJ, Gaudio AR, Berson EL. The association between visual acuity and central retinal thickness in retinitis pigmentosa. *Invest Ophthalmol Vis Sci*. 2005;46:3349–3354.
36. Biswas S, Haselier C, Mataruga A, Thumann G, Walter P, Muller F. Pharmacological analysis of intrinsic neuronal oscillations in rd10 retina. *PLoS One*. 2014;9:e99075.
37. Pennesi ME, Nishikawa S, Matthes MT, Yasumura D, LaVail MM. The relationship of photoreceptor degeneration to retinal vascular development and loss in mutant rhodopsin transgenic and RCS rats. *Exp Eye Res*. 2008;87: 561–570.
38. Augustin M, Wechdorn M, Pfeiffenberger U, et al. In vivo characterization of spontaneous retinal neovascularization in the mouse eye by multifunctional optical coherence tomography. *Invest Ophthalmol Vis Sci*. 2018;59:2054–2068.
39. Sasahara M, Otani A, Oishi A, et al. Activation of bone marrow-derived microglia promotes photoreceptor survival in inherited retinal degeneration. *Am J Pathol*. 2008;172:1693–1703.
40. Rezaei KA, Zhang Q, Chen CL, Chao J, Wang RK. Retinal and choroidal vascular features in patients with retinitis pigmentosa imaged by OCT based microangiography. *Graefes Arch Clin Exp Ophthalmol*. 2017;255:1287–1295.
41. Sugahara M, Miyata M, Ishihara K, et al. Optical coherence tomography angiography to estimate retinal blood flow in eyes with retinitis pigmentosa. *Sci Rep*. 2017;7:46396.
42. Yu DY, Cringle SJ. Retinal degeneration and local oxygen metabolism. *Exp Eye Res*. 2005;80: 745–751.
43. Padnick-Silver L, Kang Derwent JJ, Giuliano E, Narfstrom K, Linsenmeier RA. Retinal oxygenation and oxygen metabolism in Abyssinian cats with a hereditary retinal degeneration. *Invest Ophthalmol Vis Sci*. 2006;47:3683–3689.
44. Li G, De La Garza B, Shih YY, Muir ER, Duong TQ. Layer-specific blood-flow MRI of retinitis pigmentosa in RCS rats. *Exp Eye Res*. 2012;101: 90–96.
45. Stone J, Maslim J, Valter-Kocsi K, et al. Mechanisms of photoreceptor death and survival in mammalian retina. *Prog Retin Eye Res*. 1999; 18:689–735.

46. Sancho-Pelluz J, Arango-Gonzalez B, Kustermann S, et al. Photoreceptor cell death mechanisms in inherited retinal degeneration. *Mol Neurobiol*. 2008;38:253–269.
47. Penn JS, Li S, Naash MI. Ambient hypoxia reverses retinal vascular attenuation in a transgenic mouse model of autosomal dominant retinitis pigmentosa. *Invest Ophthalmol Vis Sci*. 2000;41:4007–4013.
48. Strettoi E, Pignatelli V, Rossi C, Porciatti V, Falsini B. Remodeling of second-order neurons in the retina of rd/rd mutant mice. *Vis Res*. 2003;43:867–877.
49. Jones BW, Watt CB, Frederick JM, et al. Retinal remodeling triggered by photoreceptor degenerations. *J Comp Neurol*. 2003;464:1–16.
50. Puthussery T, Taylor WR. Functional changes in inner retinal neurons in animal models of photoreceptor degeneration. *Adv Exp Med Biol*. 2010;664:525–532.
51. Jacobson SG, Sumaroka A, Aleman TS, Cideciyan AV, Danciger M, Farber DB. Evidence for retinal remodelling in retinitis pigmentosa caused by PDE6B mutation. *Br J Ophthalmol*. 2007;91:699–701.
52. Samardzija M, Wariwoda H, Imsand C, et al. Activation of survival pathways in the degenerating retina of rd10 mice. *Exp Eye Res*. 2012;99:17–26.
53. Semo M, Peirson S, Lupi D, Lucas RJ, Jeffery G, Foster RG. Melanopsin retinal ganglion cells and the maintenance of circadian and pupillary responses to light in aged rodless/coneless (rd/rd cl) mice. *Eur J Neurosci*. 2003;17:1793–1801.
54. Menzler J, Channappa L, Zeck G. Rhythmic ganglion cell activity in bleached and blind adult mouse retinas. *PLoS One*. 2014;9:e106047.
55. Milde F, Lauw S, Koumoutsakos P, Iruela-Arispe ML. The mouse retina in 3D: quantification of vascular growth and remodeling. *Integr Biol*. 2013;5:1426–1438.
56. Giannakaki-Zimmermann H, Kokona D, Wolf S, Ebneter A, Zinkernagel MS. Optical coherence tomography angiography in mice: comparison with confocal scanning laser microscopy and fluorescein angiography. *Transl Vis Sci Technol*. 2016;5:11.
57. McLenachan S, Magno AL, Ramos D, et al. Angiography reveals novel features of the retinal vasculature in healthy and diabetic mice. *Exp Eye Res*. 2015;138:6–21.
58. Salas M, Augustin M, Ginner L, et al. Visualization of micro-capillaries using optical coherence tomography angiography with and without adaptive optics. *Biomed Opt Exp*. 2017;8:207–222.